Influence of Rocky Obstacle Sand Bypassing on Embayed Beach Dynamics Using a Reduced-Complexity Shoreline Model

Elsa Durand, Bruno Castelle, Déborah Idier, Vincent Marieu, Arthur Robinet, Thomas Guérin

Journal of *Marine Science and Engineering*

MDPI

Article

Influence of Rocky Obstacle Sand Bypassing on Embayed Beach Dynamics Using a Reduced-Complexity Shoreline Model

Elsa Durand [1,2,3,*], Bruno Castelle [1], Déborah Idier [2], Vincent Marieu [1], Arthur Robinet [4] and Thomas Guérin [3]

[1] Univ. Bordeaux, CNRS, Bordeaux INP, EPOC, UMR 5805, F-33600 Pessac, France; bruno.castelle@u-bordeaux.fr (B.C.); vincent.marieu@u-bordeaux.fr (V.M.)
[2] Bureau de Recherches Géologiques et Minières (BRGM), 3 Avenue Guillemin, 45100 Orléans, France; d.idier@brgm.fr
[3] Waeles Marine Consultants, 53 rue du Commandant Groix, 29200 Brest, France; thomas.guerin@wm-consultants.fr
[4] Bureau de Recherches Géologiques et Minières (BRGM), 24 Avenue Léonard de Vinci, 33600 Pessac, France; a.robinet@brgm.fr
* Correspondence: elsa.durand@u-bordeaux.fr

Abstract: Headland and groyne sand bypassing greatly influences embayment dynamics at medium to long timescales, but is often disregarded or partially included in reduced-complexity shoreline models. This study explores how accounting for subaqueous sediment bypassing in a shoreline model affects mean embayed beach planshape and spatial variability. We implement a generic parametrization of sand bypassing in the LX-Shore model, with simulations on a synthetic embayment in two configurations: "full bypassing" (FB) where the sediments bypass the obstacle in the surfzone and beyond, and "shoreline bypassing" (SB) where bypassing occurs only when the shoreline extends beyond the obstacle. Time-invariant wave simulations show significant differences in updrift shoreline position between FB and SB. Simulations with time-varying wave angles and fixed wave height and period reveal that FB significantly impacts the embayment mean planform and spatial variability: FB reduces beach rotation by about 1/3, particularly under slightly oblique and slightly asymmetrical wave climates, and decreases shoreline curvature, especially under highly oblique wave climates. Downdrift shoreline erosion may be overestimated by up to 20% under SB. Our simulations provide new insight into the influence of subaqueous sand bypassing on embayed beach dynamics and emphasize the importance of including this process when modelling shoreline evolution in coastal embayments.

Keywords: sand bypassing; embayed beach; reduced-complexity shoreline model; equilibrium beach planform; rotation; curvature

Citation: Durand, E.; Castelle, B.; Idier, D.; Marieu, V.; Robinet, A.; Guérin, T. Influence of Rocky Obstacle Sand Bypassing on Embayed Beach Dynamics Using a Reduced-Complexity Shoreline Model. *J. Mar. Sci. Eng.* **2024**, *12*, 2266. https://doi.org/10.3390/jmse12122266

Academic Editor: Guido Benassai

Received: 29 October 2024
Revised: 28 November 2024
Accepted: 6 December 2024
Published: 10 December 2024

1. Introduction

Sandy beaches are highly dynamic coastal environments [1,2] that are under increasing demographic pressure. As an increase in beach erosion and shoreline retreat is expected in the next decades [3], a critical task for coastal scientists is to accurately predict medium- (months, years) to long-term (decades and beyond) coastal changes in order to contribute to sustainable coastal management. Embayed beaches, which are ubiquitous along the coasts worldwide [4,5], are sandy beaches delimited by physical boundaries that can be either natural rocky headlands or artificial coastal defenses. Beach morphodynamics and shoreline variability are deeply affected by these obstacles, which act both as partial or total barriers to alongshore sediment transport and are a primary control on incident wave exposure [6–13]. Therefore, embayment shorelines can exhibit a dramatic variability in their orientation and curvature from one beach to another (Figure 1) depending on wave forcing [14–17], sediment availability [18], grain size [19], obstacle size and morphology [20–22], and embayment width [5,23],

which make their evolution challenging to understand, model, and further predict. A key factor influencing embayed beach dynamics at medium to long timescales is rocky obstacle sand bypassing [24], defined as the transport of sediment around the rocky structures delimiting the embayment [5,25]. Recently, a headland bypassing classification has been proposed according to the main processes responsible for sediment transport around a headland [25]. This classification includes a differentiation between "headland bypassing swash-surfzone" (HBS), occurring when the shoreline extends up to and/or beyond the tip of the headland due to longshore transport in the swash-surfzone, and "headland bypassing surfzone/nearshore" (HBN), occurring in and seaward of the surfzone, up to the closure depth, due to nearshore subaqueous longshore transport.

Figure 1. Examples of embayed beach planforms. (**a**,**b**) Asymmetric curved beach showing large change in shoreline orientation between (**a**) November 2021 and (**b**) February 2024 due to embayment rotation at Balapitiya beach, Sri Lanka; (**c**) straight shoreline between natural headlands at Porto-Vecchio, France; (**d**) straight shoreline between artificial groynes at Palavas-les-flots, France. Images adapted from Google Earth.

Over the past few years, a new generation of reduced-complexity (also referred to as hybrid) shoreline evolution models has emerged [26–30], including models designed exclusively for embayed beaches [31,32]. Reduced-complexity shoreline models can predict wave-dominated sandy shoreline evolution on timescales ranging from hours (storms) to decades with reasonable computational cost and fairly good skill [33]. However, on embayed beaches where sand bypassing occurs, these models fail, as sand bypassing is often disregarded or only occurs when the shoreline reaches the tip of the obstacle (hereafter referred to as "shoreline bypassing" or SB), such as in LX-Shore [27]. If we refer to the classification of headland bypassing presented in [25], the initial version of the LX-Shore model considering SB was thus able to reproduce bypassing occurring in the swash zone (HBS) only, and not in the surf and nearshore zones (HBN). In [21], LX-Shore is used considering SB only and it is shown that headland length controls both the equilibrium beach planform and the spatial and temporal modes of shoreline variability at embayed beaches. However, there is field and process-based modelling evidence of subaqueous sediment bypassing (HBN in [25])

occurring within the surfzone and also further offshore [17,34–36]. There was therefore a need to improve the implementation of headland bypassing in LX-Shore, so that the model can reproduce a wider variety of headland bypassing processes (HBS and HBN). This improved implementation of bypassing in LX-Shore is hereafter referred to as "full bypassing" (FB), as opposed to the former "shoreline bypassing" (SB). ShorelineS [29] and IH-LANS [37] are some of the rare reduced-complexity shoreline model exceptions where FB is addressed, with the treatment of sand bypassing around rocky obstacles based on a bypassing factor linearly increasing and ranging from 0 to 1. In ShorelineS, this factor increases as the ratio between the depth at the tip of the structure (D_S) and the so-called depth of active longshore transport (D_{LT}) decreases, and reaches its maximum value when the shoreline reaches the tip of the obstacle [38]. In IH-LANS, this factor increases as the ratio between the headland cross-shore extent (X_H) and the surfzone width (X_S) decreases. To the best of our knowledge, the influence of these first approaches on embayed beach mean planshape and dynamics has never been explored.

Recently, improved sediment bypassing parametrizations have been proposed [17,22], which are compatible with the reduced-complexity shoreline modelling framework. Implementing these expressions in a reduced-complexity shoreline model such as LX-Shore can thus help to address the impact of obstacle sand bypassing on mean beach planform and shoreline variability at embayed coasts and provide new insight into embayed beach shoreline dynamics. In the present work, we implement the parametrization developed by McCarroll et al. (2021) [22] in the reduced-complexity shoreline model LX-Shore [27]. We investigate the sensitivity of the response of embayed beaches to the type of bypassing process implemented by comparing simulations performed considering HBS and HBN (FB configuration) versus only HBS (SB configuration). We consider an idealised coastal embayment with rectangular rocky obstacles, exposed to a range of synthetic wave climate characterised by time-invariant or time-varying angle of wave incidence.

2. Numerical Model

2.1. LX-Shore

The LX-Shore model [27] is a reduced-complexity shoreline evolution model, based on the one-line approach [39–41]. The model computes the time evolution of the sediment fraction F ranging from 0 (water) to 1 (land) within square cells (width dxy) composing of a 2D planview grid (Figure 2). Shoreline cells are those with sediment fraction $F > 0$ and an edge contact with a water cell. Partially or fully non-erodible zones are also included, such as rocky headlands where the total sediment fraction is decomposed into a fixed non-erodible fraction (rock) and a variable erodible fraction (sand). The local shoreline orientation in each shoreline cell is determined by the shore normal vector. It is assumed that the shoreline crosses this vector at a distance from the centre of the cell that depends on the sediment fraction value. The complete shoreline is then computed by interpolation of all the estimated shoreline positions. Such a 2D planview cellular-based modelling approach can thus handle complex shoreline shapes. For a detailed description of the numerical implementation and the physics involved in the model, the reader is referred to [27].

LX-Shore can account for both longshore and cross-shore sediment processes [11], which are computed using breaking wave parameters. Breaking wave conditions can be estimated either by coupling with the spectral wave model SWAN [42], or with a direct analytical formula [43], whereby the latter is used herein.

Longshore sediment transport is computed using a similar approach as in CEM and CEMSWAN models [44–47] with the empirical formula of Kamphuis (1991) [48]. Cross-shore transport is computed using an adaptation of the equilibrium-based ShoreFor model [49,50], which predicts that a translation of the beach profile in the cross-shore direction occurs when there is a disequilibrium in wave energy as the incident wave energy changes in time. Here, given that we focus on shoreline change driven by longshore processes, we consider a time-invariant offshore wave height and period in our simulations. Consequently, there

is only little temporal change in wave energy (related to time-varying wave direction in areas adjacent to the groynes and wave refraction), so cross-shore transport-driven shoreline change is assumed negligible [2] along most of the embayment, and was switched off in this study. This is further discussed in Section 4. At each time step, the sediment fraction in each shoreline grid cell ($0 < F < 1$) is thus updated based on incoming and outgoing sediment fraction caused by alongshore sediment transport.

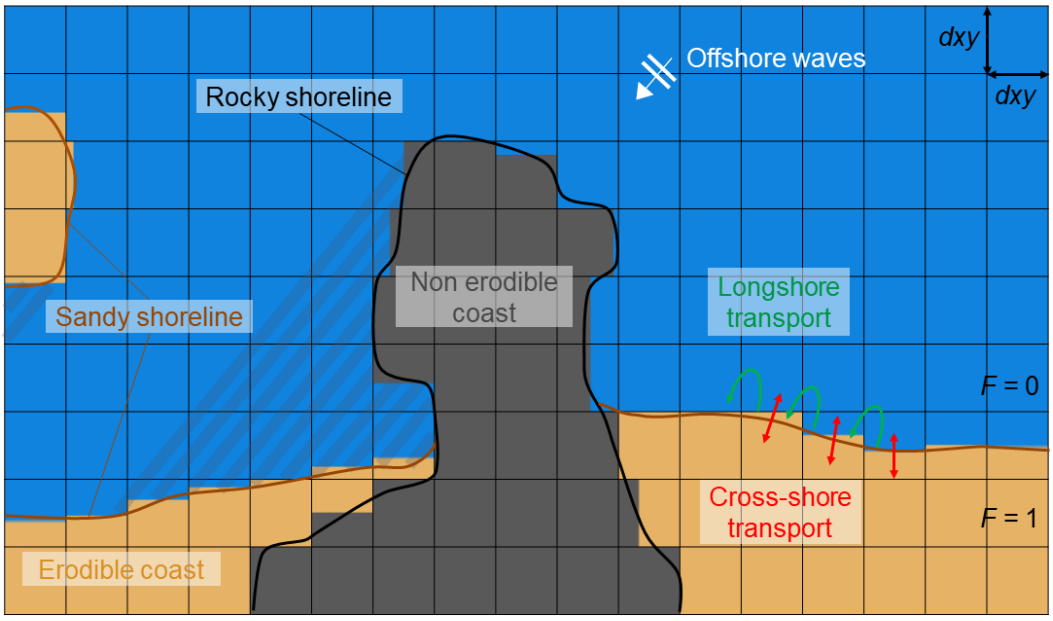

Figure 2. Schematic planview coastal area with the primary features and processes included in LX-Shore. Cross-shore transport is switched off in this study. The striped areas represent the wave shadow zones.

The main advantage of the LX-Shore model is that it enables the modelling of wave-dominated sandy shoreline evolution on large spatio-temporal scales with low computing times and good skill [11,33]. It usually takes a few minutes to a few days, depending on site complexity and computational resources, to simulate shoreline change over domains of hundreds of meters to several tens of kilometers and a duration of several decades.

2.2. Obstacle Sand Bypassing Implementation

McCarroll et al. (2021) [22] developed a parametrization of the wave-forced bypassing sediment flux around an isolated idealised headland. This expression, which has never been implemented in a reduced-complexity shoreline model before, is based on more than 1000 simulations performed with the process-based model XBeach [51] with varying waves, sediment size, or headland morphology. McCarroll et al. (2021) [22] showed that the bypassing flux Q_B (m^3/s) can be expressed as a function of the beach-scale-averaged updrift alongshore sediment flux Q_0 and the ratio between headland cross-shore extent X_H and surfzone width X_S (Figure 3):

$$Q_B = sign(A)p_1A^2 + p_2A, \quad (1)$$

where

$$A = Q_0 \exp(-b_1(X_H/X_S)^{b_2}) \quad (2)$$

and p_1, p_2, b_1, and b_2 are coefficients adjusted by calibration.

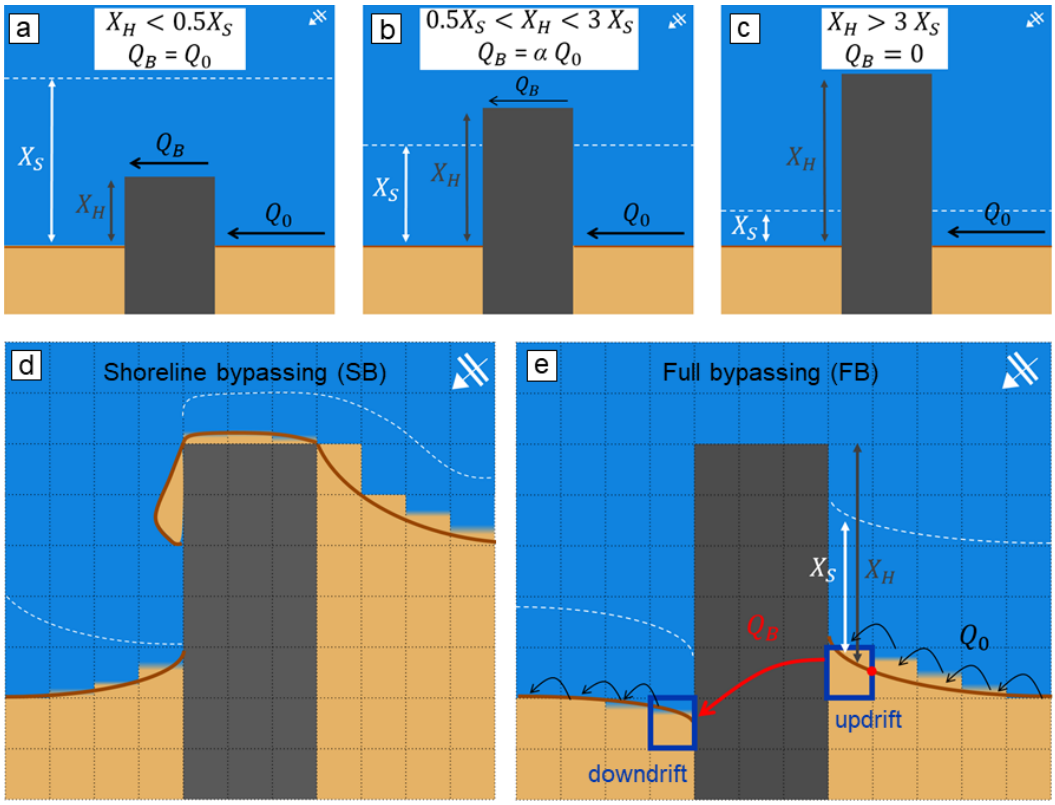

Figure 3. (**a**–**c**) Bypassing flux expression used depending on the ratio between the headland extent X_H and the surfzone width X_S. Adapted from [22]. (**d**) Schematic of the shoreline bypassing process included in the initial version of LX-Shore. (**e**) Schematic of the full bypassing implemented in the code. Sediment bypassing is transported between the two shoreline cells adjacent to each side of the obstacle (blue-framed cells) and is computed through Q_B at the updrift boundary of the updrift cell (red dot). In all panels, the dotted white line denotes the offshore limit of the surfzone.

This expression of the bypassing flux is valid for $0.5 < X_H/X_S < 3$ [22]. If $X_H/X_S < 0.5$, the obstacle is smaller than half of the surfzone and does not impact the longshore transport, and thus, $Q_B = Q_0$ (Figure 3a).

On the contrary, if $X_H/X_S > 3$, the longshore sand transport is fully blocked by the obstacle and $Q_B = 0$ (Figure 3c).

The parametrization proposed by McCarroll et al. (2021) [22] uses four free parameters calibrated on a limited range of Q_0. The parametrization is therefore well suited for a longshore flux $Q_0 \approx 1.2$ m^3/s, but results in a discontinuous distribution of the bypassing sediment flux Q_B if applied under wave conditions where $Q_0 \neq 1.2$ m^3/s without further calibration of the coefficients b_1, b_2, p_1, and p_2. In order to apply the sand bypassing parametrization to any incident wave conditions, we developed the following generic formula:

$$Q_B = \alpha Q_0 \begin{cases} \alpha = 1 \text{ if } X_H/X_S < 0.5 \\ \alpha = \exp(ax + b) - c \text{ if } 0.5 < X_H/X_S < 3 \\ \alpha = 0 \text{ if } X_H/X_S > 3 \end{cases} \quad (3)$$

with $x = X_H/X_S$.

This new expression has only one free parameter, a (since b is deduced from a and c is deduced from a and b), which has the advantage of being dimensionless. Setting $a = -2.9$ (corresponding to $b = 1.45$ and $c = 7.1 \cdot 10^{-4}$) showed the best agreement with the expression developed by McCarroll et al. (2021) [22] for $Q_0 \approx 1.2$ m^3/s (Figure 4).

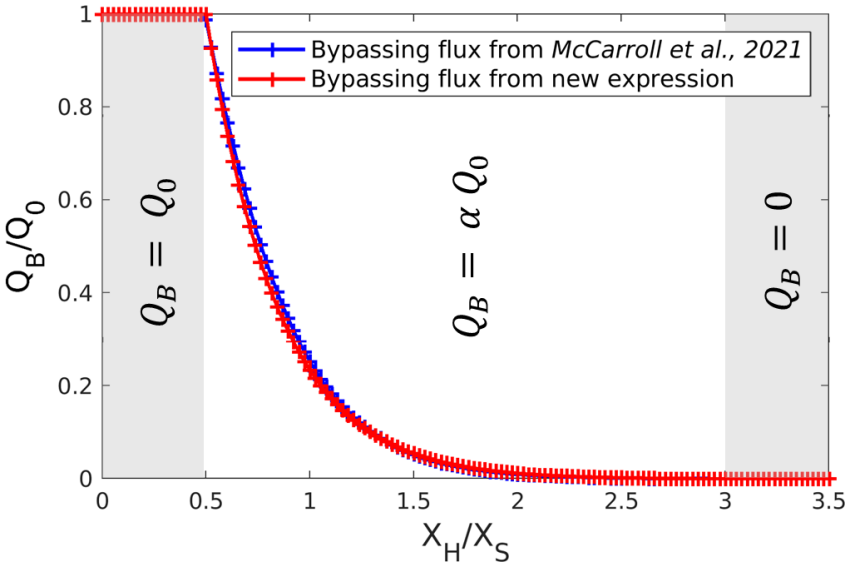

Figure 4. Bypassing flux evolution predicted with the expression given in [22] (blue) and with the new generic expression (red).

This parametrization was implemented in LX-Shore on a simple configuration consisting of an idealised straight beach with one or two rectangular rocky obstacles. In order to adapt the global approach of headland sand bypassing described in [22] to a cellular model, updrift and downdrift sandy shoreline cells adjacent to the obstacle (blue-framed cells on Figure 3e) were identified so that sediment transport could take place between these two cells even if they were not in contact spatially. The sediment bypassing flux was then computed at the updrift boundary of the updrift cell (red dot on Figure 3e) to avoid the effect of high shoreline angles at the interface between sand and rock. An automatic check was made to ensure that the tip of a rocky structure was found on the way before finding the downdrift blue cell, and the sand was finally sent to this bypassing sand receptor cell.

2.3. Stability Test of Sand Bypassing Numerical Implementation

In order to verify that the numerical implementation of the bypass works as intended, a 20-year simulation was carried out on an initially straight 10 km long beach with a rectangular 350 m long rocky headland in the centre (Figure 5a), under periodic lateral boundary conditions. The simulation was performed with a 2-hour constant time step and a grid cell size dxy of 100 m, under time-invariant wave conditions characterised by H_S = 2 m, T_P = 10 s, and θ_P = 10°, allowing for a successive observation of the different ratios X_H/X_S involved in the parametrization of the bypassing flux (Figures 3a–c and 4), without high-angle wave instabilities. At the beginning of the simulation, Q_0 is positive while the X_H/X_S ratio is high (Figure 5b), resulting in $Q_B = 0$ and a rapid accretion updrift of the obstacle and erosion downdrift. When $X_H/X_S < 3$ after approximately 2 years, Q_B starts to increase. As Q_B increases, there is less updrift accretion and downdrift erosion around the obstacle. A small accretion zone forms downdrift. Finally, when X_H/X_S = 0.5, the Q_B curve joins that of Q_0, meaning that all the sediment bypasses the obstacle. The shoreline position then gradually readjusts until it reaches an equilibrium after about 20 years. This confirms that the numerical implementation of full bypassing in LX-Shore works properly and can be further used to assess the impact of the bypass process on embayed beach planform and shoreline dynamics.

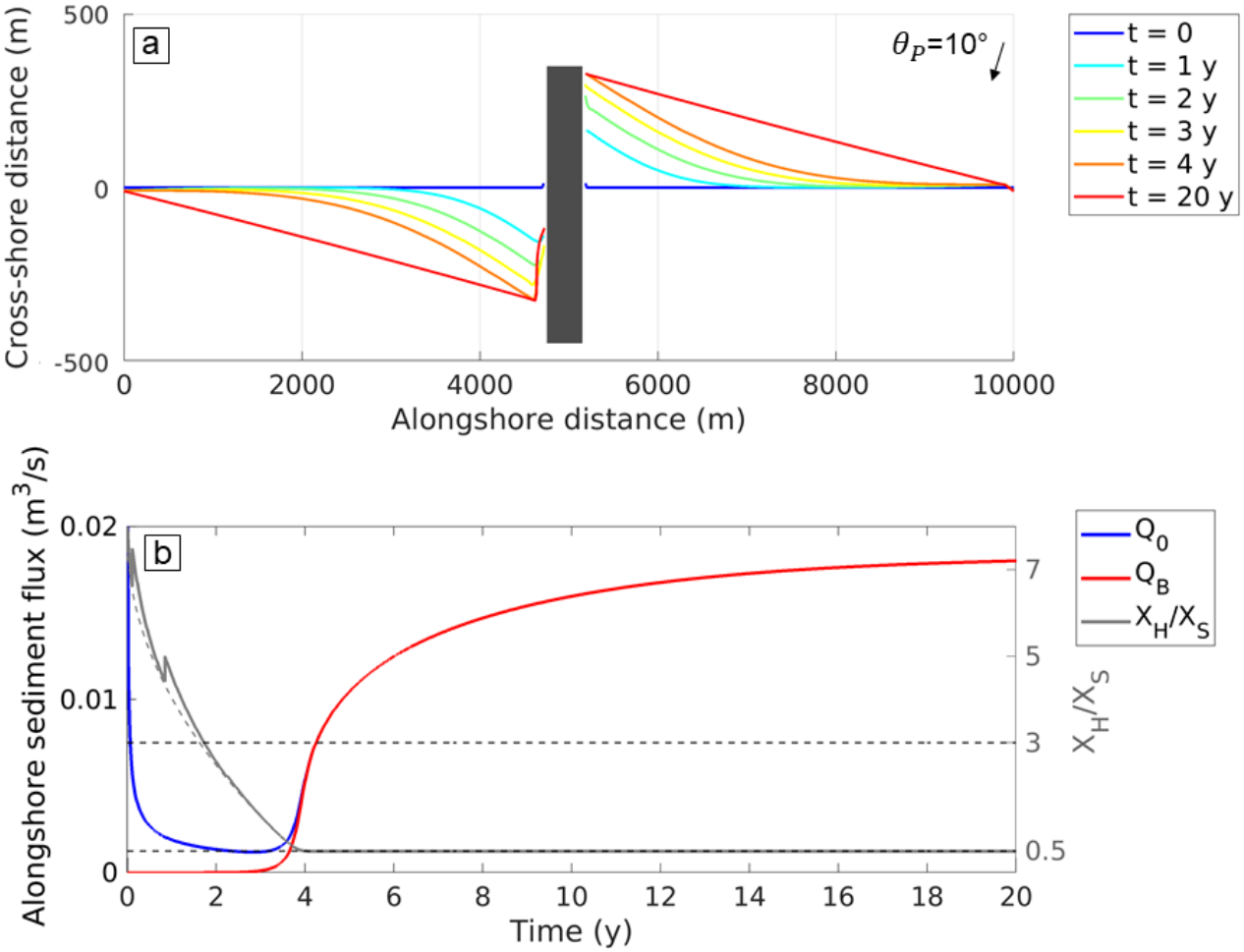

Figure 5. (**a**) Evolution of shoreline position at different time steps for a 20-year simulation. (**b**) Evolution of the bypassing (Q_B) and alongshore (Q_0) sediment fluxes superimposed onto the evolution of X_H/X_S during the simulation. The two peaks of the X_H/X_S curve at the early stage of the simulation are numerical artefacts that do not affect the overall simulation results (the curve follows its asymptote represented by the grey dashed line) caused by sand redistribution, inducing small, abrupt variations in surfzone width.

2.4. Simulation Set-Up

LX-Shore was run on an idealised 500 m long straight embayed beach with a rectangular 20 m wide and 35 m long rocky obstacle on both sides of the domain (Figure 6). The embayment dimensions were chosen so that the length of the beach met the criteria mentioned in [22]. The effect of beach length on embayment planshape and shoreline variability is further discussed in Section 4. The simulations were performed over a one-year period (simulations with stationary wave forcing), and a 5-year period (simulations with non-stationary wave forcing), with a 2-hour constant time step and a grid cell size *dxy* of 10 m. Periodic lateral boundary conditions were implemented, i.e., the sediment fraction leaving the simulation domain from the left boundary re-enters the domain from the right, and vice versa. We thus consider a circular system with a net-zero sediment budget.

For each shoreline cell, the water depth h distribution in the cross-shore direction was estimated at each time step using an equilibrium Dean profile [52] given by $h = nd^m$, where d is the offshore distance from the shoreline, $n = 0.25$ and $m = 0.67$ for the sandy profile, and $n = 0.2$ and $m = 1$ for the rocky profile. Grain size was set to D_{50} = 0.22 mm, and depth of closure to D_C = 5 m. These values correspond to orders of magnitude that are fairly common on wave-dominated sandy beaches [53,54].

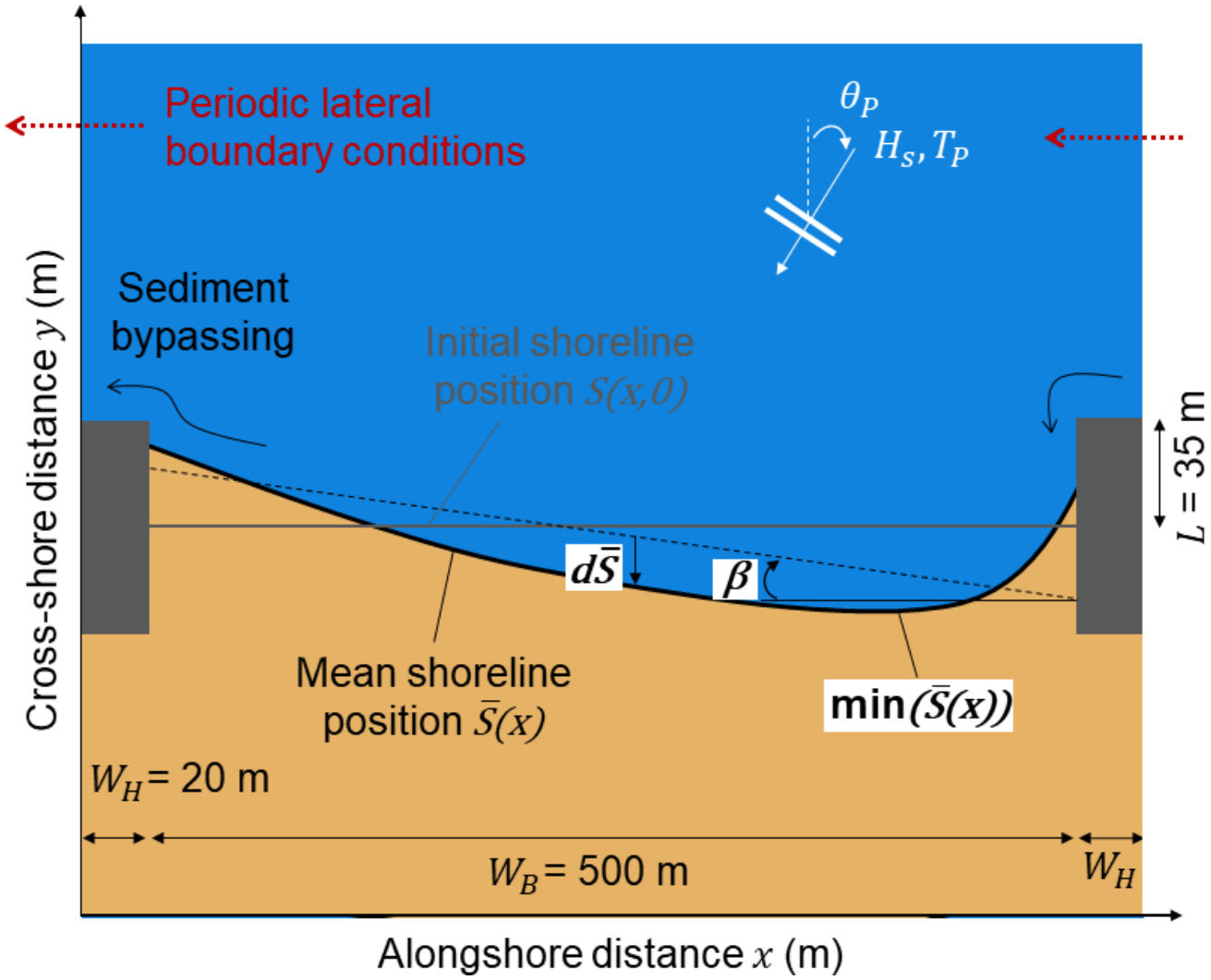

Figure 6. Schematic of embayed beach model set-up with variables used for the analysis. The black dotted line represents the mean shoreline trend-line.

In this study, breaking wave parameters were computed with the direct formula of Larson et al. (2010) [43] combined with a wave shadowing procedure. This shadowing procedure is such that cells located in areas fully protected from waves by the headland when using the direct analytical formula of Larson et al. (2010) [43] for the waves (Figure 2) can receive some sediment via longshore transport but cannot send it downdrift. This implies that, under a stationary wave climate, sand accumulates in the shadow zone without leaving it, such that the first sand cell downdrift of the shadow zone is eroding. The beach orientation readjusts in the wave-exposed zone and there is a clear breakpoint in shoreline orientation at the transition between the shadow zone and the wave-exposed zone. Under time-varying wave climates, this transition zone moves in time along the beach, leading to smooth sediment redistribution along the beach. Offshore waves were characterised by a time-invariant significant wave height H_S of 1 m and a time-invariant peak wave period T_P of 10 s, which are representative values of average swell conditions [55]. Two different sets of simulations were run: simulations with stationary wave climates (Section 3.1) with an angle of wave incidence θ_P of 10°, 20°, or 30°, and the other simulations with time-varying wave directions (Section 3.2). Following [9,15,45], for the time-varying forcing simulations, θ_P was defined by a probability distribution function (Figure 7) based on two parameters: A for the asymmetry, i.e., the fraction of waves coming from the right, and U for the obliquity, i.e., the fraction of waves approaching with high angles ($\theta_P > 45°$ or $\theta_P < -45°$).

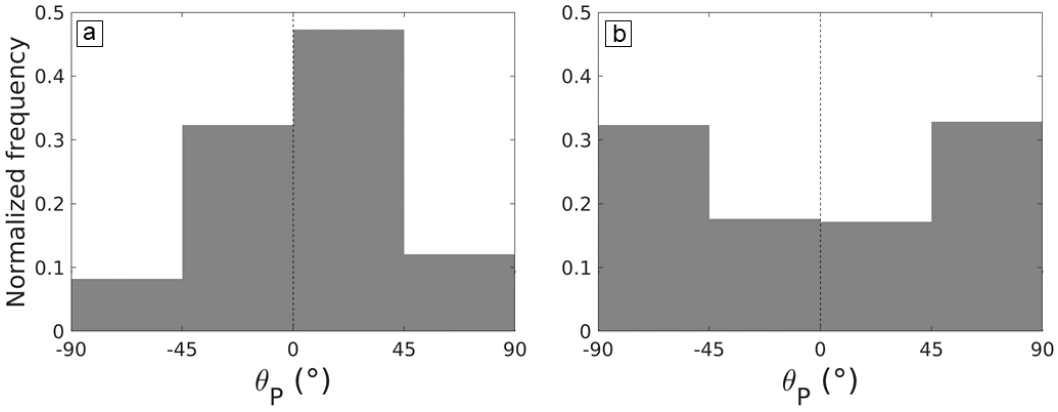

Figure 7. Frequency of occurrence of wave directions for (**a**) an asymmetric slightly oblique wave climate ($A = 0.60$, $U = 0.20$) and (**b**) a symmetric highly oblique wave climate ($A = 0.50$, $U = 0.65$).

More than 800 simulations were performed with A and U covering the entire possible range (i.e., 0 to 1) at 0.05 intervals, either considering shoreline bypassing only or full bypassing. Table 1 provides a summary of all simulation scenarios.

Table 1. Summary of the model set-up. n is the number of simulations performed for each configuration. For all simulations, we consider a constant wave height and period (H_S = 1 m and T_P = 10 s), the grid cell size is dxy = 10 m and the time step dt = 2 h. The initial rocky obstacle cross-shore extension is X_H = 35 m. Simulations shown in grey are commented in Section 4 and presented in Appendix A.

	Period	**Beach Length**	D_P	**Simulation ID**	n
Stationary wave incidence	1 year	500 m	10°	SB_St_10	1
				FB_St_10	1
			20°	SB_St_20	1
				FB_St_20	1
			30°	SB_St_30	1
				FB_St_30	1
Time-varying wave incidence	5 years	500 m	$f(A,U)$ $0<A<1$ $0<U<1$	SB_TV_500	441
				FB_TV_500	441
		250 m		SB_TV_250	441
				FB_TV_250	441
		750 m		SB_TV_750	441
				FB_TV_750	441

Simulations leading to shoreline morphodynamic instabilities [44,45], such as cuspate shorelines (Figure 8a) or flying sand spits (Figure 8b,c), that bypass the obstacles and dominate shoreline variability were disregarded in order to focus on the impact of obstacle bypassing on embayed beach rotation and curvature. In practice, it corresponds to simulations with wave climates characterised by high obliquity ($U \geq 0.60$), or to simulations where the shoreline position at the centre of the beach (x = 250 m) shows drastic changes ($\Delta y > 20$ m) within less than a week, as a sand spit or a sand wave crosses the domain.

For simulations performed with non-stationary wave climates, the first year of simulation was disregarded to avoid the effect of model spin-up from the initial shoreline that typically lasts a few months, and to focus on a shoreline variability that occurs around a true dynamic equilibrium. The mean embayed beach planform $\bar{S}(x)$ was computed over the last 4 years and shoreline variability was analysed using three different variables shown in Figure 6: mean shoreline rotation, defined as the slope of the mean shoreline trend-line (β); minimum cross-shore position of the mean shoreline (min($\bar{S}$(x)); and standard deviation of the mean shoreline relative to its trend-line ($\sigma(d\bar{S})$). The latter is further used to estimate the degree of beach curvature.

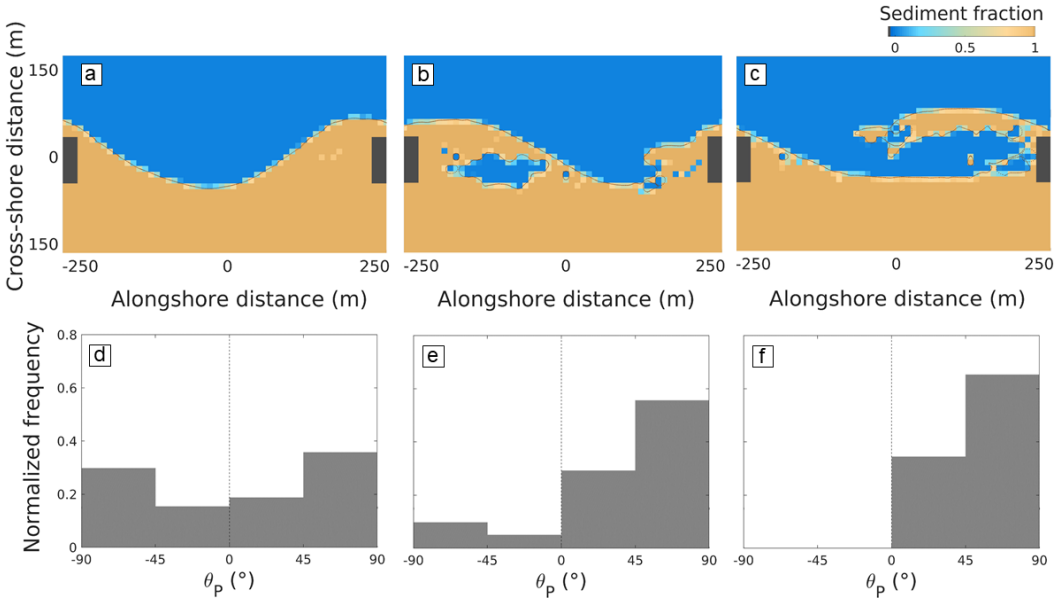

Figure 8. Beach planforms resulting from simulations performed with full bypassing (FB) under highly oblique wave climates ($U = 0.65$) with asymmetry increasing from (**a**–**c**): (**a**) $A = 0.55$, (**b**) $A = 0.85$, (**c**) $A = 1$. Panels (**d**–**f**) show the respective frequency of occurrence of wave direction θ_P for each simulation of the upper panels.

3. Results

3.1. Stationary Wave Forcing Simulations

Figure 9 shows snapshots of the embayed beach planforms after one year of simulations under time-invariant angle of wave incidence of 10° (Figure 9a,b), 20° (Figure 9c,d), and 30° (Figure 9e,f). For simulations performed only with shoreline bypassing (SB) (top panels), the shoreline reaches the updrift tip of the obstacle and passes around the obstacle, resulting in a small accumulation of sand downdrift, with shoreline bulge size increasing with increasing wave angle.

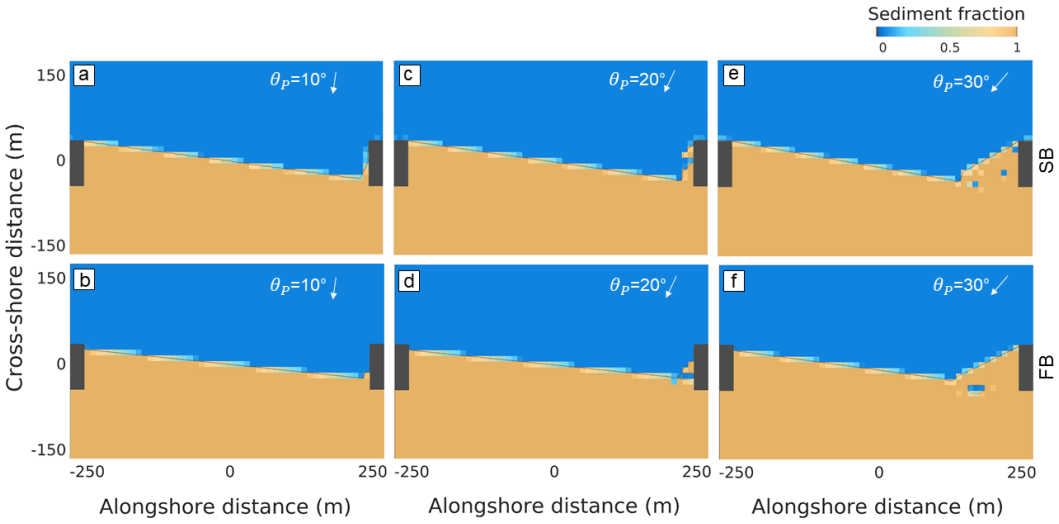

Figure 9. Embayed beach planforms after one year for stationary wave angles of 10°, 20°, and 30° with (**a**,**c**,**e**) shoreline bypassing only (SB_St_10, SB_St_20, and SB_St_30) and (**b**,**d**,**f**) full bypassing (FB_St_10, FB_St_20, and FB_St_30).

For simulations performed with full bypassing (FB), the shoreline saturates approximately 10 m before the tip of the structure because it reaches the point where $X_H/X_S \approx 0.5$. At this point, $Q_B = Q_0$ and all the sand transported by the longshore drift bypasses the

obstacle and reaches the downdrift coast. A similar bulge as the one observed in SB mode forms a downdrift of the obstacle as the bypassing sand accumulates behind it. The presence of this bulge is further discussed in Section 4. Our results indicate that considering subaqueous sand bypassing (FB) has a substantial influence on the shoreline morphology updrift of headlands. The shoreline cross-shore position updrift of the obstacle under FB can be reduced by approximately 30% compared to shoreline position obtained in SB simulations.

3.2. Time-Varying Wave Forcing Simulations

Figure 10 shows the time-averaged shoreline position (black line) and envelope (grey area) for all time-varying wave simulations performed considering shoreline bypassing only (Figure 10a) and full bypassing (Figure 10b). Simulations under the red dotted line were further excluded from the analysis due to shoreline morphodynamic instabilities as explained in Section 2. Overall, mean shorelines under full bypassing readily show less rotation, milder curvature and a less extreme maximum of erosion. This indicates that improving the description of sand bypassing substantially affects the mean coastal embayment planform, whatever the obliquity and asymmetry of the wave climate. This is further quantified in Figure 11, which also provides more insight into the wave climate conditions under which the impact of the newly implemented full bypassing is the strongest.

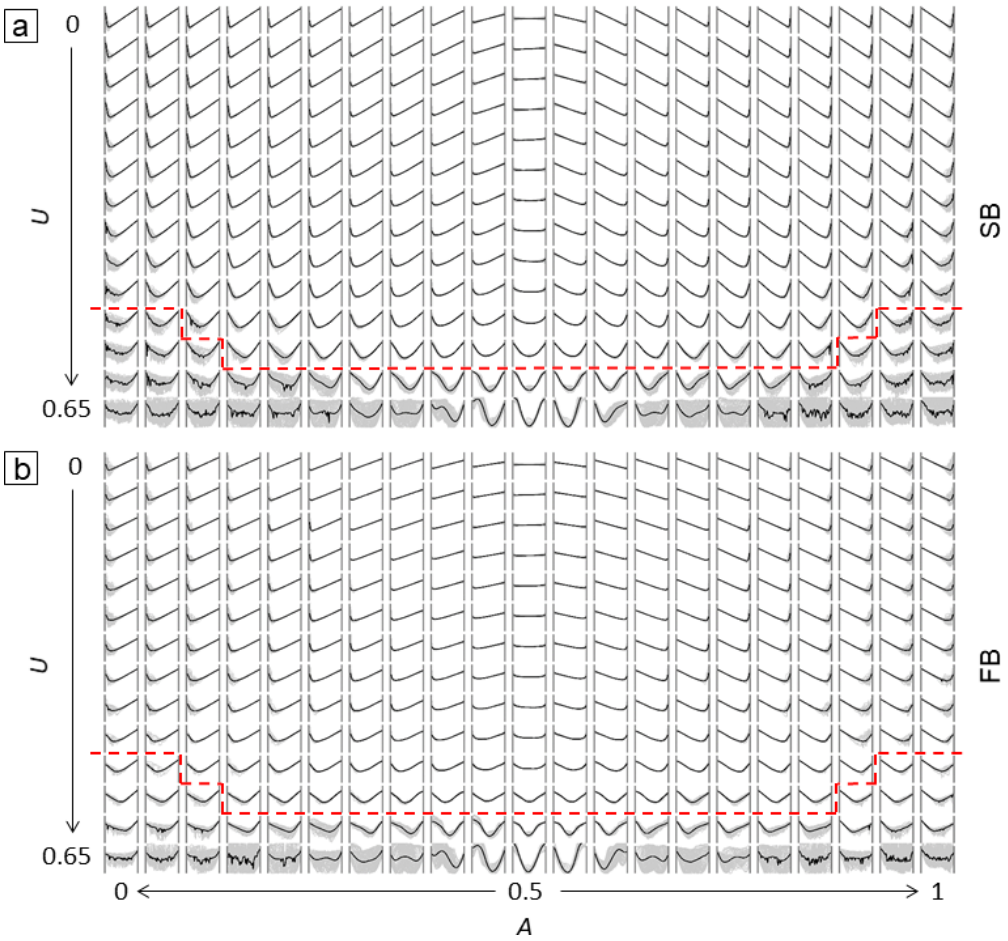

Figure 10. Overview of mean shoreline planform (black line) and envelope (grey area) for each simulation with varying obliquity, U, and asymmetry, A, of wave incidence, with (**a**) only shoreline bypassing (SB_TV_500) and (**b**) full bypassing (FB_TV_500). The vertical black lines at both sides of the shoreline represent the two rocky obstacles. Simulations under the red dotted line are disregarded in the analysis (see Section 2).

Under shoreline bypassing (SB), shoreline rotation β ranges approximately between $-7°$ and $+7°$ (Figure 11a), while it ranges from $-5°$ to $+5°$ under full bypassing (FB, Figure 11b). In both cases, β is higher for wave climates characterised by high asymmetry and low obliquity (top left and top right areas on Figure 11a,b). Indeed, as wave obliquity increases, more sand bypasses (both SB and FB) and is distributed along the beach through alongshore drift, resulting in less embayment rotation. The most significant impact of full bypassing is observed under slightly asymmetric and slightly oblique wave climates (most colorful squares near the top centre of Figure 11c), with a difference of about 2.5° for β, showing a reduction in shoreline rotation by approximately 33% under FB. These simulations are those for which shoreline bypassing (SB) does not occur, but full bypassing (FB) does. On the contrary, the implementation of FB shows the least impact for simulations characterised by symmetric wave climates, or by high asymmetry and high obliquity (white squares in Figure 11c). In the first case, waves coming alternately from left and right may lead to a compensation between sand bypassing in both directions under FB, resulting in a similar shoreline shape as when no sand is bypassing under SB. In the second case, a lot of sand already bypasses the obstacle under SB as the shoreline often reaches the tip of the structure, and thus, FB implementation shows only little effect on the embayment planform.

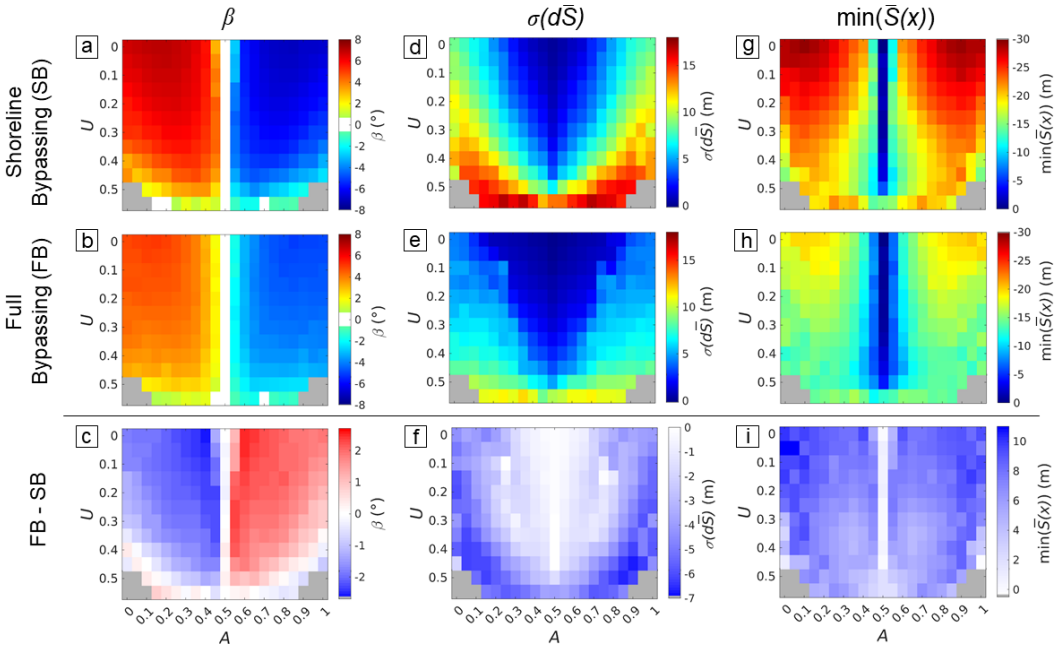

Figure 11. (**a**–**c**) Mean shoreline rotation β for (**a**) shoreline bypassing (SB_TV_500) and (**b**) full bypassing (FB_TV_500); (**c**) difference in β values between FB and SB. (**d**–**f**) Standard deviation of $d\bar{S}$ for (**d**) SB and (**e**) FB; (**f**) difference in $\sigma(d\bar{S})$ values between FB and SB. (**g**–**i**) Minimum y position of mean shoreline for (**g**) SB and (**h**) FB; (**i**) difference in minimum shoreline position values between FB and SB.

Maximum values of the standard deviation of the mean shoreline relative to its trendline $\sigma(d\bar{S})$, used to estimate beach curvature, are observed for simulations performed with highly asymmetrical and highly oblique wave climates. These values reach about 17 m for shoreline bypassing (SB) (Figure 11d), compared to 14 m for full bypassing (FB, Figure 11e). Maximum differences in $\sigma(d\bar{S})$ between FB and SB reach 3 to 4 m, showing a reduction in beach curvature by approximately 20% under FB, and occur for simulations characterised by moderately to highly asymmetrical wave incidence (sharp blue squares on Figure 11f). In such a situation, a lot of sand bypasses the obstacle under SB, resulting in sand accumulations against the rocky structures on both sides of the beach, which are not observed with FB. For the other simulations, ($0.3 < A < 0.7$) embayed beach curvature is reduced by approximately 1 to 2 m with full bypassing.

With shoreline bypassing only (SB), minimum shoreline values (min($\bar{S}$(x))) range from −20 m to −35 m (Figure 11g), while the major part of the values ranges between −15 m and −25 m for full bypassing (FB) (Figure 11h). Maximum differences in min($\bar{S}$(x)) between FB and SB reach 8 m, meaning a reduction in the most eroded shoreline position by approximately 20%. Under SB only, erosion around the rocky obstacle is thus increased. The impact of FB on maximum erosion is relatively uniform across wave climates, with a slightly greater impact in the case of slightly oblique and moderately asymmetrical wave climates (deeper blue areas in Figure 11i).

Figure 12 provides an overview of the magnitude of the differences between shorelines predicted by simulations performed with SB only (dotted line) and with FB (continuous line) for three of the simulations, leading to the most significant differences between SB and FB.

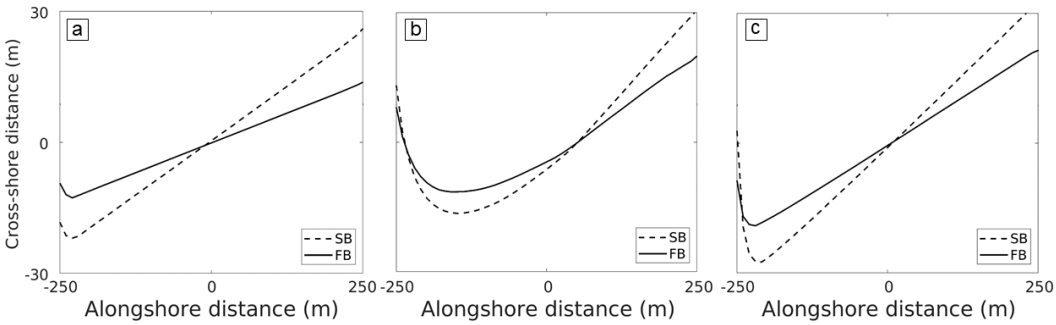

Figure 12. Mean embayed beach planform for simulations showing large differences between SB (dotted line) and FB (continuous line) in terms of (**a**) beach rotation ($A = 0.40$, $U = 0$), (**b**) curvature ($A = 0.30$, $U = 0.45$), and (**c**) maximum of erosion ($A = 0.20$, $U = 0.05$).

On a 500 m long beach, mean shoreline position updrift and downdrift of the obstacle can be about 10 m different between simulations performed with SB and FB (Figure 12a), as well as the cross-shore position of maximum of erosion (Figure 12c) under slightly oblique wave climates. In such a case, as there is no shoreline bypassing (SB), but subaqueous bypassing (FB) occurs, the accretion updrift of the obstacle and the erosion downdrift are maximised in SB mode, and so is rotation. Shoreline curvature is also strongly impacted in the presence of FB (Figure 12b). Under highly oblique wave climates, more sand accumulates along the obstacles under SB than under FB, leading to greater erosion at the centre of the beach. Under FB, more sand is distributed along the beach, which is therefore less curved than under SB only.

4. Discussion

It has long been acknowledged that natural or artificial coastal structures disturb the longshore drift and can deeply affect the coastal embayment planshape on a wide range of space- and timescales [18]. For instance, on timescales of months to years, coastal engineering structures such as groynes can be used to adjust the shoreline position [56] and protect coastal areas and associated stakes. On longer (geological) timescales, natural headlands readily control the coastal landscapes along rugged coasts [10,24]. Thus, the degree of sand transport bypassing the obstacle must be carefully included in shoreline change models. Our simulations indicate that using a more comprehensive implementation of rocky obstacle bypassing impacts both mean embayment planshape and shoreline spatial variability. Figure 12 provides a clear illustration of the potential magnitude of the impact of the consideration of subaqueous bypassing (FB) on shoreline rotation, curvature, and the landward maximum cross-shore position compared to SB only. These findings are in line with earlier work showing that sediment bypassing is critical for embayment mean planform and dynamics [21,24,34]. In addition, while mean embayed beach planform empirical models can represent real bay shapes found in nature [57], some of them fail to reproduce shoreline shape downdrift of relatively short rocky obstacles, as shown in [13].

Such a difference can be attributed to headland subaqueous sand bypassing. Further, only one beach length was investigated in Section 3. However, the impact of subaqueous bypassing on embayment planshape and shoreline variability can vary according to the length of the beach. Additional simulations were performed (see Appendix A) on the same configuration as those presented in Figure 6 but with different beach lengths. The results indicate that the impact of FB on beach rotation increases with decreasing beach length. On the contrary, the impact of FB on maximum localised erosion increases with increasing beach length. The length of the beach tested was generally short, but as we also consider a short rocky obstacle length, the criteria presented by McCarroll et al. (2021) [22] for applying the bypassing expression are met. The ratio between the embayment length and the cross-shore extent of the rocky obstacle exceeds 5 [58], and the ratio between the beach length and the surfzone width exceeds 10 [5,6]. The alongshore current has thus room to fully develop between the rocky obstacles, and the assumption of disregarding cross-shore processes is tenable.

This work builds on recent advances on obstacle sand bypassing processes [25] and the recent development of reduced-complexity shoreline models [26–30]. Such an approach arises as an efficient and computationally cheap alternative to process-based models describing the evolution of embayed beaches (e.g., [8,21]), although some processes are disregarded, such as, e.g., the coupling with the nearshore sandbars [59]. The modelling framework proposed herein using the generic bypassing flux expression developed by McCarroll et al. (2021) [22] can be applicable to other reduced-complexity models, e.g., CoSMoS-COAST [26], COCOONED [28], or the model of Tran et al. (2020) [60]. McCarroll et al. (2021) [22] mentioned that direct observations of headland bypassing volumes for validation are rare to non-existent. However, they conducted a validation test against one of the few observational studies of bypassing made at Start Bay, UK. The results suggest that their Q_B expression provides a reasonable first-pass estimate of real-world bypassing volumes around small idealised headlands. Further calibration, including assessments of this formulation for more complex morphologies and larger-scale headlands would require additional field observations. As it is based on a large number of process-based model runs, this formulation may be more appropriate physically than those already implemented in other models, where the bypassing flux linearly increases as the ratio D_S/D_{LT} (ShorelineS, [29]) or X_H/X_S (IH-LANS, [37]) decreases. As the formulation used in IH-LANS is based on the same variables as the one presented in [22], further tests were carried out to compare our approach against that used in IH-LANS. Simulations were run (not shown) on the same configuration as the one described in Figure 6, but using the expression of the bypassing flux used by Alvarez-Cuesta et al. (2021) [37]. The results show that both formulations are broadly equivalent for slightly asymmetrical wave climates ($0.3 < A < 0.7$). However, they show greater differences in terms of rotation, curvature, and maximum erosion for highly asymmetrical wave climates. In case of such wave climates, rotation is maximised (see Figure 11b), so X_H is small and the situation where $X_H/X_S < 0.5$ is more frequent. In LX-Shore, using the bypassing flux expression adapted from [22], when this threshold is reached, $Q_B = Q_0$, so the entire sediment flux bypasses the rocky obstacle. The formulation presented in [37] does not include this threshold, and the bypassing flux continues to increase until $X_H = 0$. This highlights the importance of this threshold $X_H/X_S = 0.5$, which is the primary difference with the expressions used in IH-LANS and ShorelineS. The formulation proposed by McCarroll et al. (2021) [22] assumes an idealised headland shape, but additional process-based simulations can be performed to derive more generic bypassing formulas, such as the one presented in [17] that considers several other parameters largely impacting the amount of sediment bypassing (e.g., headland size and shape, but also tide or subtidal bathymetry). The development of such parametrizations should be encouraged, going with the general objective to apply reduced-complexity models to a wider range of environments and to further reduce model result uncertainties.

In the version of the model presented here, in FB mode, the shoreline can only extend beyond the rocky structure in the situation of HAWI (high-angle wave instabilities; see

Figure 8). It is not clear whether and under which conditions (excluding HAWI) the shoreline can extend beyond the tip of the obstacle in nature, but a possible extension of the model to allow such behaviour would be to switch to SB when the sediment fraction in the sandy cells around the tip of the structure exceeds an arbitrary threshold (e.g., 0.95). Such shoreline extending beyond the tip of the headland may also occur on tidal beaches where SB can eventually occur at low tide, which may favour further shoreline accretion and further, under certain conditions, lead to SB at all tide stages.

Most of the reduced-complexity modelling exercises focused on simulations without sediment bypassing or shoreline bypassing only (e.g., [9,21]). Our work has the potential to be extended to real beaches in order to better explore the impact of FB on the different modes of shoreline variability. Such real beach applications will require using spectral wave modelling, which is possible in the present framework as LX-Shore can be coupled to the SWAN [42] model (see, for instance, [11]). Accounting for more complex embayed beach configurations may also require further developments, including, for instance, more complex headland geometries and other headland proxies, e.g., headland toe depth [22], to compute sand bypassing fluxes. To our knowledge, there is no field evidence of a sand bulge as large as that observed downdrift of the obstacle in Figure 9e,f. The presence of this bulge (not observed in most of the non-stationary simulations) may be due to the use of stationary wave climates, which does not exist in nature. Furthermore, we use the formula of Larson et al. (2010) [43], which does not properly reproduce wave refraction along non-parallel bathymetric iso-contours. Therefore, the use of more realistic wave climates and a spectral wave model could also enable a more accurate prediction of shoreline position downdrift of the headland. Moreover, in FB mode, the bypassing sand is considered to be transported directly into the cell immediately downdrift of the obstacle. In reality, the sand may move further downdrift depending on the incident wave conditions. Allowing the sand to be deposited further downdrift of the obstacle could also improve the agreement of the modelled shoreline with observations immediately downdrift of the obstacle.

5. Conclusions

A generic parametric expression for wave-forced rocky obstacle sand bypassing based on the work of McCarroll et al. (2021) [22] was implemented for the first time in a reduced-complexity shoreline model, LX-Shore. This new implementation enables the model to account for a broader range of sediment bypassing processes, including bypassing occurring seaward of the surfzone. The impact of this improved implementation (named here "full bypassing" or FB) compared to the previous one ("shoreline bypassing" or SB) on embayed beach planform and shoreline dynamics was investigated through simulations considering a synthetic embayed beach under a wide variety of wave climates with constant wave height and period and varying asymmetry and obliquity. Accounting for FB instead of only SB has a substantial influence on embayed beach rotation, curvature, and most landward cross-shore shoreline position. Specifically, the impact of better accounting for obstacle sediment bypassing on beach rotation is particularly significant under slightly oblique and slightly asymmetric wave climates, where the angle of beach rotation is reduced by approximately 1/3 compared to SB. Concerning beach curvature, the impact of considering FB is greater under highly asymmetrical wave forcing. The maximum shoreline erosion downdrift of the structure can also be overestimated by up to 20% considering only SB instead of FB. Our results provide general trends in the behaviour of embayed beaches in the presence/absence of subaqueous headland sand bypassing. This work encourages further quantitative local assessments by applying such reduced-complexity modelling approaches to real sites, using headland bypassing parametrizations derived from process-based models and field measurements.

Author Contributions: Conceptualization, E.D., B.C., D.I. and T.G.; methodology, B.C., D.I., T.G., E.D., V.M. and A.R.; software, E.D., V.M. and A.R.; formal analysis, E.D. and B.C.; investigation, E.D.; writing—original draft preparation, E.D.; writing—review and editing, B.C., D.I., T.G., A.R., V.M. and E.D.; visualization, E.D. and A.R.; project administration, B.C., D.I. and T.G.; funding acquisition, B.C., D.I. and T.G. All authors have read and agreed to the published version of the manuscript.

Funding: This work was funded in the scope of an ANRT/CIFRE contract (n°2021/0579) between Waeles Marine Consultants, Bordeaux University and BRGM, and was performed in the frame of the SHORMOSAT ANR project (grant n° ANR-21-CE01-0015).

Institutional Review Board Statement: Not applicable.

Informed Consent Statement: Not applicable.

Data Availability Statement: The raw data supporting the conclusions of this article will be made available by the authors on request.

Conflicts of Interest: The authors declare no conflicts of interest. The funders had no role in the design of the study; in the collection, analyses, or interpretation of data; in the writing of the manuscript; or in the decision to publish the results.

Appendix A. Effect of Beach Length on Differences in Shoreline Position Obtained in SB and FB Modes

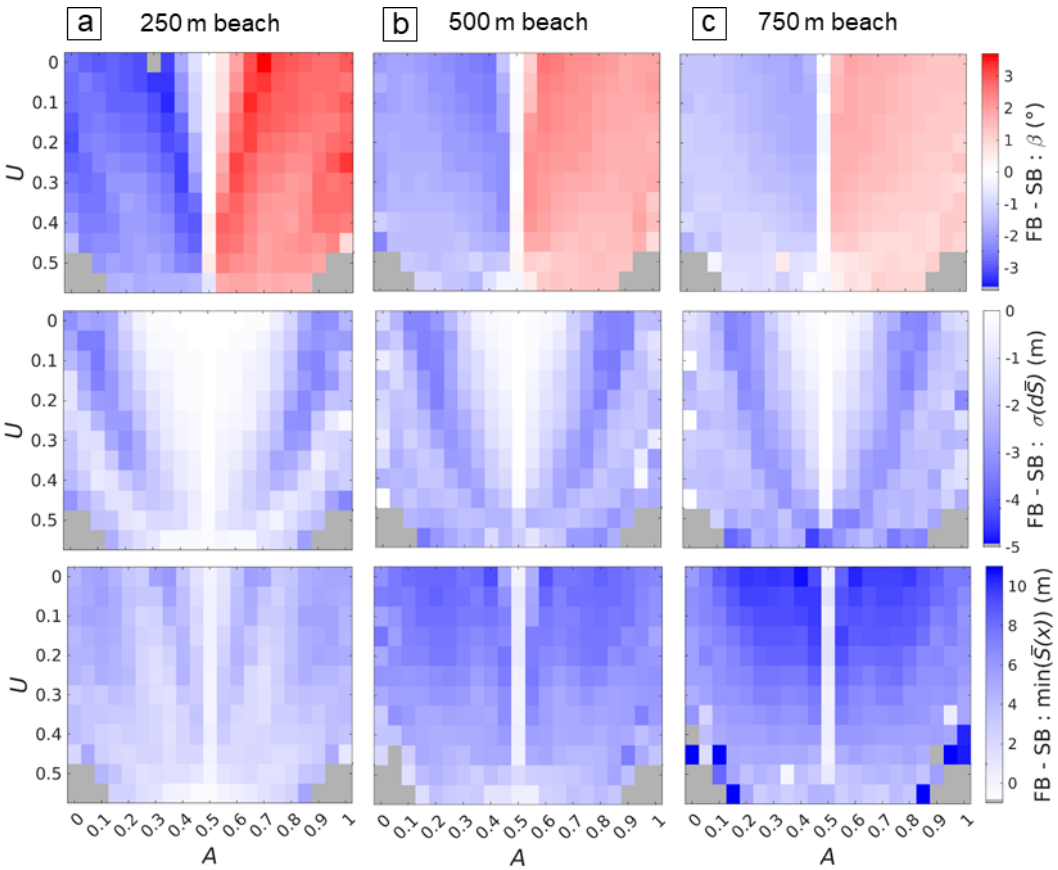

Figure A1. Distribution of the differences in β, $\sigma(d\bar{S})$, and $min(\bar{S})$ between FB and SB for (**a**) a 250 m beach (FB_TV_250—SB_TV_250), (**b**) a 500 m beach (FB_TV_500—SB_TV_500), and (**c**) a 750 m beach (FB_TV_750—SB_TV_750).

References

1. Wright, L.; Short, A. Morphodynamic variability of surf zones and beaches: A synthesis. *Mar. Geol.* **1984**, *56*, 93–118. [CrossRef]
2. Castelle, B.; Masselink, G. Morphodynamics of wave-dominated beaches. *Camb. Prism. Coast. Futur.* **2023**, *1*, e1. [CrossRef]
3. Vousdoukas, M.I.; Ranasinghe, R.; Mentaschi, L.; Plomaritis, T.A.; Athanasiou, P.; Luijendijk, A.; Feyen, L. Sandy coastlines under threat of erosion. *Nat. Clim. Chang.* **2020**, *10*, 260–263. [CrossRef]
4. Inman, D.L.; Nordstrom, C.E. On the Tectonic and Morphologic Classification of Coasts. *J. Geol.* **1971**, *79*, 1–21. [CrossRef]
5. Short, A.D.; Masselink, G. Structurally Controlled Beaches. In *Handbook of Beach and Shoreface Morphodynamics*; JohnWiley and Sons Ltd.: Hoboken, NJ, USA, 1999; pp. 230–250.
6. Castelle, B.; Coco, G. The morphodynamics of rip channels on embayed beaches. *Cont. Shelf Res.* **2012**, *43*, 10–23. [CrossRef]
7. Turki, I.; Medina, R.; Gonzalez, M.; Coco, G. Natural variability of shoreline position: Observations at three pockets beaches. *Mar. Geol.* **2013**, *338*, 76–89. [CrossRef]
8. Daly, C.J.; Bryan, K.R.; Winter, C. Wave energy distribution and morphological development in and around the shadow zone of an embayed beach. *Coast. Eng.* **2014**, *93*, 40–54. [CrossRef]
9. Ratliff, K.M.; Murray, A.B. Modes and emergent time scales of embayed beach dynamics. *Geophys. Res. Lett.* **2014**, *41*, 7270–7275. [CrossRef]
10. Fellowes, T.E.; Vila-Concejo, A.; Gallop, S.L. Morphometric classification of swell-dominated embayed beaches. *Mar. Geol.* **2019**, *411*, 78–87. [CrossRef]
11. Robinet, A.; Castelle, B.; Idier, D.; Harley, M.; Splinter, K. Controls of local geology and cross-shore/longshore processes on embayed beach shoreline variability. *Mar. Geol.* **2020**, *422*, 106118. [CrossRef]
12. Fellowes, T.E.; Vila-Concejo, A.; Gallop, S.L.; Harley, M.D.; Short, A.D. Wave shadow zones as a primary control of storm erosion and recovery on embayed beaches. *Geomorphology* **2022**, *399*, 108072. [CrossRef]
13. Nobre Silva, A.; Taborda, R.; Andrade, C. Embayed beach configuration explained by wave sheltering. *Sci. Rep.* **2024**, *14*, 1099. [CrossRef] [PubMed]
14. Harley, M.D.; Turner, I.L.; Short, A.D. New insights into embayed beach rotation: The importance of wave exposure and cross-shore processes. *J. Geophys. Res. Earth Surf.* **2015**, *120*, 1470–1484. [CrossRef]
15. Hurst, M.D.; Barkwith, A.; Ellis, M.A.; Thomas, C.W.; Murray, A.B. Exploring the sensitivities of crenulate bay shorelines to wave climates using a new vector-based one-line model: Sensitivity of crenulate bays. *J. Geophys. Res. Earth Surf.* **2015**, *120*, 2586–2608. [CrossRef]
16. Vieira da Silva, G.; Toldo, E.E., Jr.; Klein, A.H.d.F.; Short, A.D. The influence of wave-, wind- and tide-forced currents on headland sand bypassing—Study case: Santa Catarina Island north shore, Brazil. *Geomorphology* **2018**, *312*, 1–11. [CrossRef]
17. King, E.V.; Conley, D.C.; Masselink, G.; Leonardi, N.; McCarroll, R.J.; Scott, T.; Valiente, N.G. Wave, Tide and Topographical Controls on Headland Sand Bypassing. *J. Geophys. Res. Ocean.* **2021**, *126*. [CrossRef]
18. Da Silva, A.P.; Vieira Da Silva, G.; Strauss, D.; Murray, T.; Woortmann, L.G.; Taber, J.; Cartwright, N.; Tomlinson, R. Headland bypassing timescales: Processes and driving forces. *Sci. Total Environ.* **2021**, *793*, 148591. [CrossRef]
19. McCarroll, R.; Masselink, G.; Valiente, N.; Scott, T.; King, E.; Conley, D. Wave and Tidal Controls on Embayment Circulation and Headland Bypassing for an Exposed, Macrotidal Site. *J. Mar. Sci. Eng.* **2018**, *6*, 94. [CrossRef]
20. George, D.A.; Largier, J.L.; Pasternack, G.B.; Barnard, P.L.; Storlazzi, C.D.; Erikson, L.H. Modeling Sediment Bypassing around Idealized Rocky Headlands. *J. Mar. Sci. Eng.* **2019**, *7*, 40. [CrossRef]
21. Castelle, B.; Robinet, A.; Idier, D.; D'Anna, M. Modelling of embayed beach equilibrium planform and rotation signal. *Geomorphology* **2020**, *369*, 107367. [CrossRef]
22. McCarroll, R.J.; Masselink, G.; Valiente, N.G.; King, E.V.; Scott, T.; Stokes, C.; Wiggins, M. An XBeach derived parametric expression for headland bypassing. *Coast. Eng.* **2021**, *165*, 103860. [CrossRef]
23. Ab Razak, M.S.B.A. Natural Headland Sand Bypassing: Towards Identifying and Modelling the Mechanisms and Processes. Ph.D. Thesis, Delft University of Technology, Delft, The Netherlands, 2015.
24. Goodwin, I.D.; Freeman, R.; Blackmore, K. An insight into headland sand bypassing and wave climate variability from shoreface bathymetric change at Byron Bay, New South Wales, Australia. *Mar. Geol.* **2013**, *341*, 29–45. [CrossRef]
25. Klein, A.H.; Vieira da Silva, G.; Taborda, R.; da Silva, A.P.; Short, A.D. Headland bypassing and overpassing: Form, processes and applications. In *Sandy Beach Morphodynamics*; Elsevier: Amsterdam, The Netherlands, 2020; pp. 557–591. [CrossRef]
26. Vitousek, S.; Barnard, P.L.; Limber, P.; Erikson, L.; Cole, B. A model integrating longshore and cross-shore processes for predicting long-term shoreline response to climate change: CoSMoS-COAST. *J. Geophys. Res. Earth Surf.* **2017**, *122*, 782–806. [CrossRef]
27. Robinet, A.; Idier, D.; Castelle, B.; Marieu, V. A reduced-complexity shoreline change model combining longshore and cross-shore processes: The LX-Shore model. *Environ. Model. Softw.* **2018**, *109*, 1–16. [CrossRef]
28. Antolínez, J.A.A.; Méndez, F.J.; Anderson, D.; Ruggiero, P.; Kaminsky, G.M. Predicting Climate-Driven Coastlines with a Simple and Efficient Multiscale Model. *J. Geophys. Res. Earth Surf.* **2019**, *124*, 1596–1624. [CrossRef]
29. Roelvink, D.; Huisman, B.; Elghandour, A.; Ghonim, M.; Reyns, J. Efficient Modeling of Complex Sandy Coastal Evolution at Monthly to Century Time Scales. *Front. Mar. Sci.* **2020**, *7*, 535. [CrossRef]

30. Alvarez-Cuesta, M.; Losada, I.; Toimil, A. A nearshore evolution model for sandy coasts: IH-LANSloc. *Environ. Model. Softw.* **2023**, *169*, 105827. [CrossRef]
31. Turki, I.; Medina, R.; Coco, G.; Gonzalez, M. An equilibrium model to predict shoreline rotation of pocket beaches. *Mar. Geol.* **2013**, *346*, 220–232. [CrossRef]
32. Jaramillo, C.; Jara, M.S.; González, M.; Medina, R. A shoreline evolution model for embayed beaches based on cross-shore, planform and rotation equilibrium models. *Coast. Eng.* **2021**, *169*, 103983. [CrossRef]
33. Montaño, J.; Coco, G.; Antolínez, J.A.A.; Beuzen, T.; Bryan, K.R.; Cagigal, L.; Castelle, B.; Davidson, M.A.; Goldstein, E.B.; Ibaceta, R.; et al. Blind testing of shoreline evolution models. *Sci. Rep.* **2020**, *10*, 2137. [CrossRef]
34. Vieira da Silva, G.; Toldo, E.E.; Klein, A.H.d.F.; Short, A.D.; Woodroffe, C.D. Headland sand bypassing—Quantification of net sediment transport in embayed beaches, Santa Catarina Island North Shore, Southern Brazil. *Mar. Geol.* **2016**, *379*, 13–27. [CrossRef]
35. Valiente, N.G.; Masselink, G.; Scott, T.; Conley, D.; McCarroll, R.J. Role of waves and tides on depth of closure and potential for headland bypassing. *Mar. Geol.* **2019**, *407*, 60–75. [CrossRef]
36. Mouragues, A.; Bonneton, P.; Castelle, B.; Marieu, V.; Jak McCarroll, R.; Rodriguez-Padilla, I.; Scott, T.; Sous, D. High-Energy Surf Zone Currents and Headland Rips at a Geologically Constrained Mesotidal Beach. *J. Geophys. Res. Ocean.* **2020**, *125*, e2020JC016259. [CrossRef]
37. Alvarez-Cuesta, M.; Toimil, A.; Losada, I. Modelling long-term shoreline evolution in highly anthropized coastal areas. Part 1: Model description and validation. *Coast. Eng.* **2021**, *169*, 103960. [CrossRef]
38. Ghonim, M. Recent Developments in Numerical Modelling of Coastline Evolution, Advanced Development and Evaluation of ShorelineS Coastline Model. Master's Thesis, IHE: Delft, The Netherlands, 2019.
39. Pelnard-Considère, R. Essai de théorie de l'évolution des formes de rivage en plages de sable et de galets. *Journees de L'hydraulique* **1957**, *4*, 289–298.
40. Komar, P.D.; Inman, D.L. Longshore sand transport on beaches. *J. Geophys. Res.* **1970**, *75*, 5914–5927. [CrossRef]
41. Hanson, H.; Kraus, N.C. *GENESIS: Generalized Model for Simulating Shoreline Change*; Coastal Engineering Research Center: Vicksburg, MS, USA, 1989.
42. Booij, N.; Ris, R.C.; Holthuijsen, L.H. A third-generation wave model for coastal regions: 1. Model description and validation. *J. Geophys. Res. Ocean.* **1999**, *104*, 7649–7666. [CrossRef]
43. Larson, M.; Hoan, L.X.; Hanson, H. Direct Formula to Compute Wave Height and Angle at Incipient Breaking. *J. Waterw. Port Coastal, Ocean. Eng.* **2010**, *136*, 119–122. [CrossRef]
44. Ashton, A.; Murray, A.B.; Arnoult, O. Formation of coastline features by large-scale instabilities induced by high-angle waves. *Nature* **2001**, *414*, 296–300. [CrossRef]
45. Ashton, A.D.; Murray, A.B. High-angle wave instability and emergent shoreline shapes: 1. Modeling of sand waves, flying spits, and capes. *J. Geophys. Res.* **2006**, *111*, F04011. [CrossRef]
46. Valvo, L.M.; Murray, A.B.; Ashton, A. How does underlying geology affect coastline change? An initial modeling investigation. *J. Geophys. Res. Earth Surf.* **2006**, *111*, 2005JF000340. [CrossRef]
47. Limber, P.W.; Adams, P.N.; Murray, A.B. Modeling large-scale shoreline change caused by complex bathymetry in low-angle wave climates. *Mar. Geol.* **2017**, *383*, 55–64. [CrossRef]
48. Kamphuis, J.W. Alongshore Sediment Transport Rate. *J. Waterw. Port Coastal Ocean. Eng.* **1991**, *117*, 624–640. [CrossRef]
49. Davidson, M.A.; Splinter, K.D.; Turner, I.L. A simple equilibrium model for predicting shoreline change. *Coast. Eng.* **2013**, *73*, 191–202. [CrossRef]
50. Splinter, K.D.; Turner, I.L.; Davidson, M.A.; Barnard, P.; Castelle, B.; Oltman-Shay, J. A generalized equilibrium model for predicting daily to interannual shoreline response. *J. Geophys. Res. Earth Surf.* **2014**, *119*, 1936–1958. [CrossRef]
51. Roelvink, D.; Reniers, A.; Van Dongeren, A.; Van Thiel De Vries, J.; McCall, R.; Lescinski, J. Modelling storm impacts on beaches, dunes and barrier islands. *Coast. Eng.* **2009**, *56*, 1133–1152. [CrossRef]
52. Dean, R.G. Equilibrium Beach Profiles: Characteristics and Applications. *J. Coast. Res.* **1991**, *7*, 53–84.
53. Komar, P.D. *Beach Processes and Sedimentation*, 2nd ed.; Prentice Hall: Upper Saddle River, NJ, USA, 1998.
54. Athanasiou, P.; Van Dongeren, A.; Giardino, A.; Vousdoukas, M.; Gaytan-Aguilar, S.; Ranasinghe, R. Global distribution of nearshore slopes with implications for coastal retreat. *Earth Syst. Sci. Data* **2019**, *11*, 1515–1529. [CrossRef]
55. Holthuijsen, L.H. *Waves in Oceanic and Coastal Waters*; Cambridge University Press: Cambridge, UK, 2007.
56. Kristensen, S.; Drønen, N.; Deigaard, R.; Fredsoe, J. Impact of groyne fields on the littoral drift: A hybrid morphological modelling study. *Coast. Eng.* **2016**, *111*, 13–22. [CrossRef]
57. Hsu, J.R.C.; Yu, M.J.; Lee, F.C.; Benedet, L. Static bay beach concept for scientists and engineers: A review. *Coast. Eng.* **2010**, *57*, 76–91. [CrossRef]
58. Scott, T.; Austin, M.; Masselink, G.; Russell, P. Dynamics of rip currents associated with groynes — field measurements, modelling and implications for beach safety. *Coast. Eng.* **2016**, *107*, 53–69. [CrossRef]

59. Blossier, B.; Bryan, K.R.; Daly, C.J.; Winter, C. Shore and bar cross-shore migration, rotation, and breathing processes at an embayed beach. *J. Geophys. Res. Earth Surf.* **2017**, *122*, 1745–1770. [CrossRef]
60. Tran, Y.H.; Barthélemy, E. Combined longshore and cross-shore shoreline model for closed embayed beaches. *Coast. Eng.* **2020**, *158*, 103692. [CrossRef]